Materials Horizons

ROYAL SOCIETY OF CHEMISTRY

COMMUNICATION

View Article Online
View Journal | View Issue

Cite this: *Mater. Horiz.*, 2020, 7, 1828

Received 5th March 2020,
Accepted 14th April 2020

DOI: 10.1039/d0mh00394h

rsc.li/materials-horizons

Bio-inspired transparent MXene electrodes for flexible UV photodetectors†

Jiaxin Chen, Ziliang Li, Fenglou Ni, Weixin Ouyang and Xiaosheng Fang *

2D transition metal carbides (MXenes) have emerged as one of the representative materials for transparent electrodes of electronics, but it is still a challenge to achieve highly transparent and conductive MXene electrodes for flexible photodetectors due to the tradeoff between resistance and transmittance. Herein, we put forward a bio-inspired transparent MXene film with a high transmittance of about 90% and low sheet resistance value of around 3 Ω sq^{-1}. Moreover, thanks to the presence of various surface terminal groups, the MXene electrode's work function is adjustable *via* different etching processes, and in conjunction with electrospun TiO_2 films a semi-transparent UV photodetector is integrated. Furthermore, the electrode and the constructed photodetector both exhibit superb flexibility which can survive 1000 bending cycles. This work not only provides a novel pathway to simultaneously improve the transmittance and conductivity of transparent electrodes, but also is available for extensive applications of optoelectronics.

New concepts

As a sort of rising two dimensional materials, MXenes have huge potential for they not only possess superb electrical conductivity and high hydrophilicity, but also enjoy mechanical strength and flexibility. Yet their applications to optoelectronics as electrodes are limited owing to the tradeoff between high transmittance and low resistance, as a low resistance needs more conductive materials, reducing the light transmission by producing a larger surface coverage. To tackle this bottleneck, here a novel bio-inspired strategy is reported to acquire transparent flexible electrodes with both high transparency and high conductivity which outperform other transparent electrodes. The electrode simultaneously exhibits reliable flexibility during a series of mechanical tests. All these properties of the MXene electrodes result from the well-designed hierarchical leaf vein network structure and strong adhesion between the MXene and urea-treated substrates. In applications, a free-standing semi-transparent UV photodetector is constructed using the MXene electrodes, showing high-performance UV detection as well as superb flexibility and stability. The method provides a new route for MXene based optoelectronics.

Transparent flexible electrodes are an essential part in optoelectronic devices such as solar cells, light emitting diodes (LEDs), and photodetectors, which are generally supposed to possess high electrical conductivity for efficient carrier transport as well as high optical transmittance for negligible light shading. Photodetectors, which convert light into electrical signals, have additional requirements for electrodes of work function matching to realize Schottky or Ohmic contacts.

A considerable number of different electrode materials have been reported, commonly being fabricated into transparent compact thin films or meshed networks.[1] Among the varieties available, indium tin oxide (ITO) is the most frequently used transparent electrode, yet the inherent brittleness hinders its potential applications of wearable and flexible electronics. As for newly developed Ag nanowires, they have excellent conductivity but their work function is constrained in a limited range. Moreover, the inadequate hydrophilicity possibly excludes their extensive applicability to form a rather uniform film on many substrates. The up-and-coming graphene films are transferred *via* a complex process which may introduce polymer impurities, and furthermore there is still room for improving their conductivity. To make efficient use of incident light, a transparent flexible electrode with the advantages of high conductivity and facile preparation is required to offer an indispensable component for future optoelectrical devices.

MXenes are a promising class of materials with broad applications in energy storage,[2] sensors,[3] electromagnetic interference shielding,[4] photodetection,[5,6] lasers,[7] medical treatment,[8] electrocatalytic conversion[9] and so on. $Ti_3C_2T_x$ is the first discovered and the most widely studied MXene material,[10–12] which possesses extraordinary electrical conductivity, hydrophilicity, mechanical strength and other intriguing properties.[13,14] It is found that the work function of $Ti_3C_2T_x$ can be modulated in a very wide range from 2.14 eV to 5.65 eV through surface termination modification, winning out over metal electrodes by providing a wide choice of Schottky or Ohmic contacts.[15–18] These qualities of $Ti_3C_2T_x$ make it

Department of Materials Science, Fudan University, Shanghai 200438, China. E-mail: xshfang@fudan.edu.cn

† Electronic supplementary information (ESI) available. See DOI: 10.1039/d0mh00394h

suitable for being used as electrodes that demand high conductivity, transparency and adjustable work function as well as flexibility, along with the rise of wearable and transplantable electronics. However, although $Ti_3C_2T_x$ can be used as transparent electrodes, it seems difficult to achieve both high transparency and high conductivity.[19–23] For example, Zhang and co-workers fabricated transparent and flexible MXene films whose transmittance reached as high as 95% but the sheet resistance (R_s) was 1032 Ω sq^{-1}.[13] There are only a few reported flexible photodetectors with MXene electrodes.[5] MXene films that can further break the tradeoff between low R_s and high transmittance across the UV-vis-NIR spectrum as well as have the potential for being applied to flexible photodetectors have received little attention, inspiring this study.

The objective of this report is to develop transparent flexible MXene electrodes with excellent mechanical strength. Recently, new designs of leaf vein-based transparent electrodes have been reported.[24] It is proved that the leaf venation networks enjoy effective current collection of the surface and minimum in-plane resistance.[1] In this report we describe the use of bio-inspired leaf vein networks coated with a MXene film layer as the electrodes of flexible UV photodetectors for the first time. The following advantages can be achieved through our design: (1) electrodes with superior optical transmittance and low sheet resistance; (2) outstanding flexibility as well as dependable mechanical strength; (3) tunable work functions matching different photodetectors; and (4) free-standing and lightweight properties for potential wearable electronics.

Our electrode was made from a *myrica rubra* leaf (Fig. 1a). First the mesophyll was etched in hot alkali solution and the leaf veins would survive the etching process. Then the dried veins were coated with a layer of dark conducting $Ti_3C_2T_x$ (named m-$Ti_3C_2T_x$) slurry, which was synthesized through the minimally intensive layer delamination (MILD) method.[25] Full process details can be found in the ESI.† As seen from Fig. 1b, the process perfectly keeps the network structure of the leaf veins and m-$Ti_3C_2T_x$ conformally covers the whole leaf surface. Fig. 1c shows the enlarged image of restacked m-$Ti_3C_2T_x$ layers, which have wrinkles and clear edges. The transmission electron microscopy (TEM) image of a single layer of m-$Ti_3C_2T_x$ with no wrinkles confirms that its size extends to several micrometers (Fig. 1e). Fig. 1f suggests that m-$Ti_3C_2T_x$ has good crystallinity.

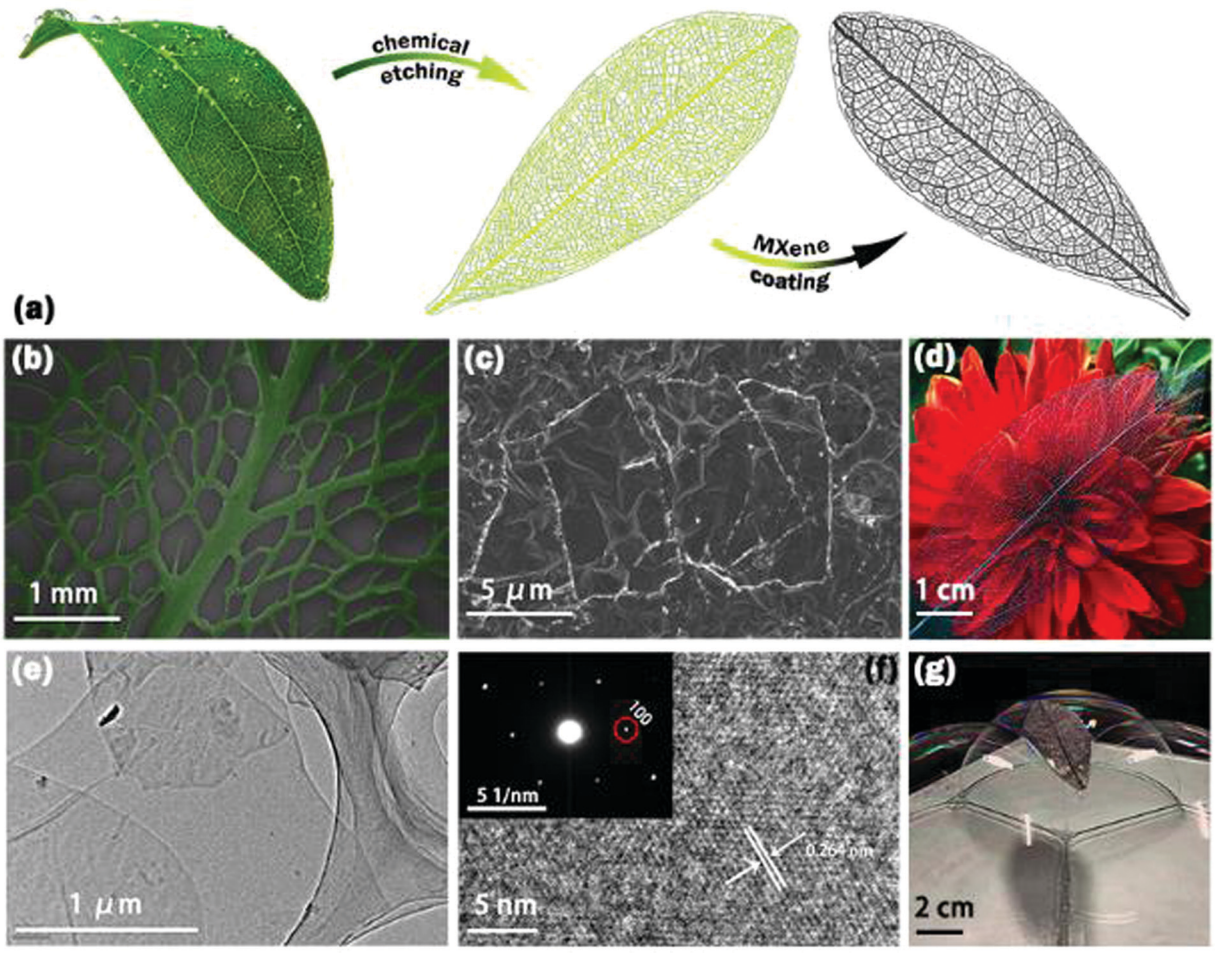

Fig. 1 (a) Schematic illustration of the synthesis process of leaf-based electrodes. (b) SEM image of a leaf-based electrode coated with m-$Ti_3C_2T_x$. (c) Enlarged SEM image of m-$Ti_3C_2T_x$ films. (d) Optical image of leaf-based electrodes over a flower. (e) TEM image of single layer of m-$Ti_3C_2T_x$. (f) HRTEM and SAED images of few-layered m-$Ti_3C_2T_x$. (g) Photo of a leaf-based electrode on soap suds.

To give a better display of how this network structure can be used as flexible electrodes, the m-$Ti_3C_2T_x$ leaf is put above a flower and Fig. 1d clarifies its high transparency. What's more, the free-standing leaf electrode is so lightweight that it can stay steady even when placed upon soap bubbles (Fig. 1g).

As the coating time increases, the leaf weighs more, which can be evidenced by the $\Delta m/m_0$ values (m_0 is the original weight of a leaf without MXene slurry, and Δm is the gained weight of the leaf after each coating of MXene slurry) in Fig. 2a. The increasing weight indicates that there is more MXene adhering to the leaf surface, and R_s decreases to about 3 Ω sq^{-1} after coating MXene for 8 times. The morphology of the leaf electrodes is shown in Fig. S1 (ESI†), demonstrating that the leaf veins are uniformly coated with a layer of MXene as the coating times increase. To show the adjustable conductivity of the leaf electrode, we also coated the leaf vein with MXene solutions of varying m-$Ti_3C_2T_x$ contents and the sheet resistance values are also shown in Fig. S2 (ESI†). The electrode exhibits high transparency over a broad spectrum. From Fig. 2b, it is apparent that the electrode keeps a high transmittance of nearly 90% in the whole UV-visible range. In addition, the transmittance does not change with the increased coating times under illumination of different wavelengths. The electrode also has superb flexibility and mechanical strength. As seen from Fig. 2c, electrodes with different conductivity were realized according to Fig. S2 (ESI†), where MXene solutions with less $Ti_3C_2T_x$ sheets than those in the MXene slurry were applied. The sheet resistance of the electrodes remains stable after being bent at 180° for 1000 times. The electrode morphology after different bending cycles is shown in Fig. S3 (ESI†), demonstrating that the MXene layers on the leaf veins show no obvious change after the bending tests, which also confirms that the electrode has excellent flexibility and stability.

This flexibility may result from the strong adhesion force between the MXene and the leaf surface. To strengthen the interaction between the leaf and MXene, during the fabrication process, the leaves were immersed in urea solution before being coated with the MXene. It is proved that there exist strong bonds between urea and the surface groups of the MXene (–O–, –F, and –OH),[26] and the organic compositions of the leaf veins also absorb urea molecules.[27] To test the adhesion force between the leaf and MXene, a Scotch Tape adhesion test was carried out

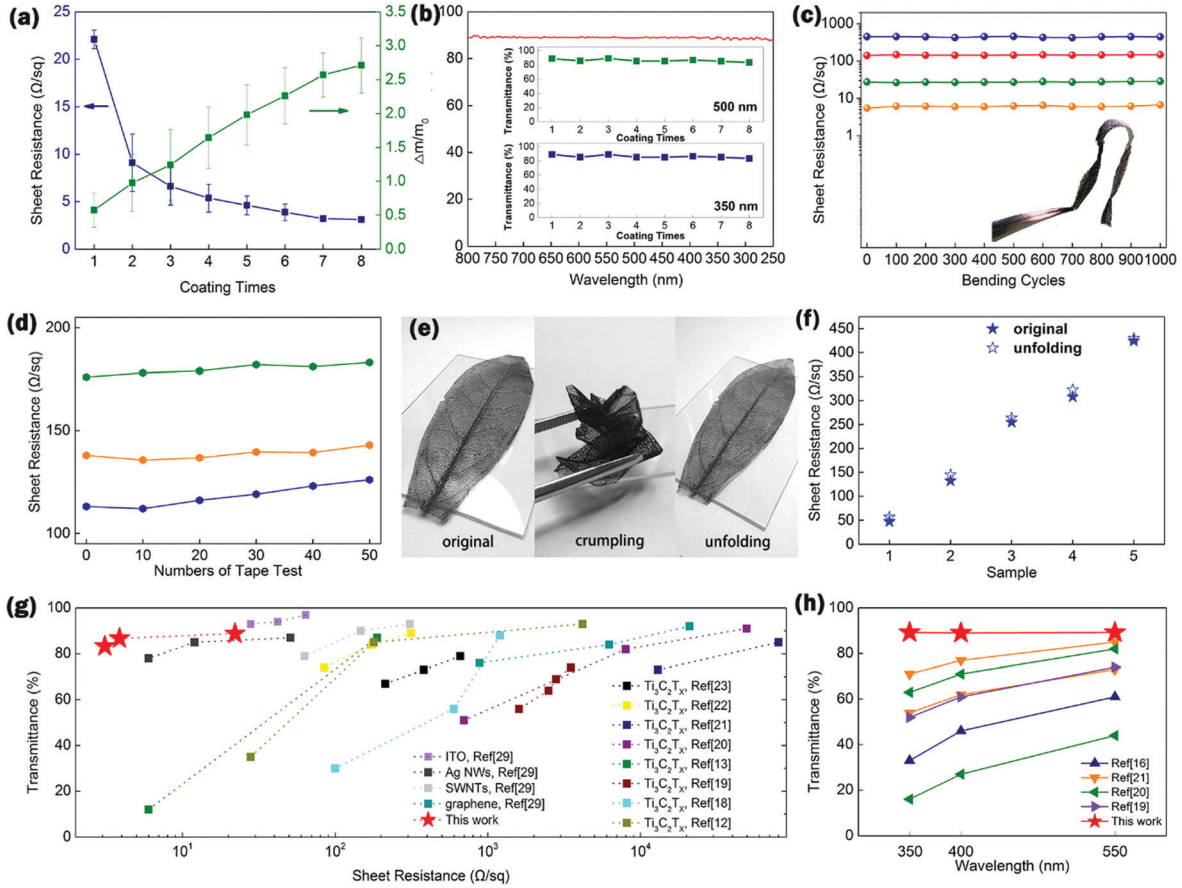

Fig. 2 (a) The relationship between sheet resistance values as well as $\Delta m/m_0$ and coating times. (b) The transmittance spectra of the m-$Ti_3C_2T_x$ leaf electrode. The inset image depicts the transmittance change over the coating time. (c) The sheet resistance values of the leaf electrode after being bent at 180°. (d) The sheet resistance values of leaf electrodes during tape tests. (e) Optical images of leaf-based electrodes before crumpling, during crumpling and after unfolding. (f) The sheet resistance before crumpling and after unfolding. (g) The transmittance and sheet resistance of different transparent conductive films. (h) The transmittance at 350 nm, 400 nm and 550 nm of various transparent conductive films.

and as seen in Fig. 2d the electrode could survive 50 cycles of sticking and peeling and the sheet resistance value was more stable than other transparent electrodes.[28] The surface after different test cycles is shown in Fig. S4 (ESI†), indicating that after 50 cycles the MXene layer is still uniformly coated on the leaf vein surface. The electrode also exhibits excellent stability while being crumpled. Fig. 2e shows the crumpling and unfolding process. The electrode could recover to the original flat shape after unfolding and the sheet resistance value stayed almost unchanged (Fig. 2f). The scanning electron microscopy (SEM) images before crumpling and after unfolding are shown in Fig. S5 (ESI†), indicating that during the test the MXene layer closely adheres to the leaf surface. As seen in Fig. 2g, the leaf-based electrode outperforms a lot of $Ti_3C_2T_x$-based transparent conductive films in both sheet resistance values and transmittance (at 550 nm). What's more, it shows advantages over some electrodes including ITO, Ag nanowires (Ag NWs), single-walled carbon nanotubes (SWNTs) and graphene film.[29] Fig. 2h depicts their transmittance at fixed wavelengths of 350, 400 and 550 nm. The transmittance of the listed other $Ti_3C_2T_x$-based transparent films dramatically decreases over the UV range, while our electrode not only has higher transmittance over the visible range but also keeps a high value under UV irradiation, demonstrating its potential for optoelectronics, especially applications in the UV range.

The as-fabricated electrodes can be used in a flexible UV photodetector as a free-standing electrode with high transparency and conductivity. To achieve electrodes with different work functions, $Ti_3C_2T_x$ synthesized by HF etching and TBAOH intercalation method (named h-$Ti_3C_2T_x$) was used. As seen from Fig. 3a, at first a slit was made in the processed leaf veins and two types of MXenes (m-$Ti_3C_2T_x$ and h-$Ti_3C_2T_x$) were coated onto different parts. h-$Ti_3C_2T_x$ showed a slighter color than m-$Ti_3C_2T_x$. Before the evaporation of solvent in the MXene layers, a lightweight electrospun TiO_2 thin film was stuck on the leaf electrode and the two were gently pressed together, thus forming a flexible free-standing photodetector. During the photoeletrical tests, two probes were placed onto two different parts of the leaf electrode (m-$Ti_3C_2T_x$ and h-$Ti_3C_2T_x$).

It can be seen from SEM images that the slit is several micrometers wide (Fig. 3c). The TiO_2 film (Fig. 3b) clings to the leaf resulting in tight contact between the semiconductor and the conductor. The enlarged SEM image depicts the illumination area during the tests (Fig. 3d), where two probes are placed on both sides and electrospun TiO_2 can be clearly seen. It is confirmed through Raman and X-ray diffraction (XRD) spectra that the synthesized TiO_2 is of the anatase phase (Fig. S6, ESI†). The morphology details of multilayer h-$Ti_3C_2T_x$ are shown in an SEM image and the accordion-like particles indicate the successful etching of MAX, which is the characteristic morphology of the HF-etched MXene (Fig. 3e).[30] The TEM image of h-$Ti_3C_2T_x$ is shown in Fig. S7 (ESI†) where the high-resolution transmission electron microscopy (HRTEM) and selected area electron diffraction (SAED) results indicate good crystallinity of h-$Ti_3C_2T_x$. Note that the leaf electrode coated with h-$Ti_3C_2T_x$ also shows high transparency over a wide spectrum range (Fig. S8, ESI†).

The surface chemistry of the two kinds of $Ti_3C_2T_x$ was characterized through X-ray photoelectron spectroscopy (XPS) data as shown in Fig. S9 and S10 (ESI†), which demonstrated the presence of terminal groups. It is worth noting that the XPS spectra indicate that there is a clear difference in the atomic percentage between m-$Ti_3C_2T_x$ and h-$Ti_3C_2T_x$ (Table S1, ESI†), indicating their different surface chemistry. When the MAX phase was etched by the MILD process, the –F groups on the $Ti_3C_2T_x$ surface are more than the –O functional terminals, while the opposite occurs during HF + TBAOH etching. XRD characterization as shown in Fig. S11 (ESI†) was used to analyze the formation and crystalline nature of the MXene. The appearance of almost only one intense (002) peak with an increased intensity at 6.0° (m-$Ti_3C_2T_x$) and 5.7° (h-$Ti_3C_2T_x$) demonstrated the successful removal of Al elements during the two kinds of etching processes. The surface functional groups can be characterized through Raman spectra as well (Fig. S12, ESI†).

The free-standing photodetector shows an obvious photoresponse under UV illumination (Fig. 4a); the on/off ratio

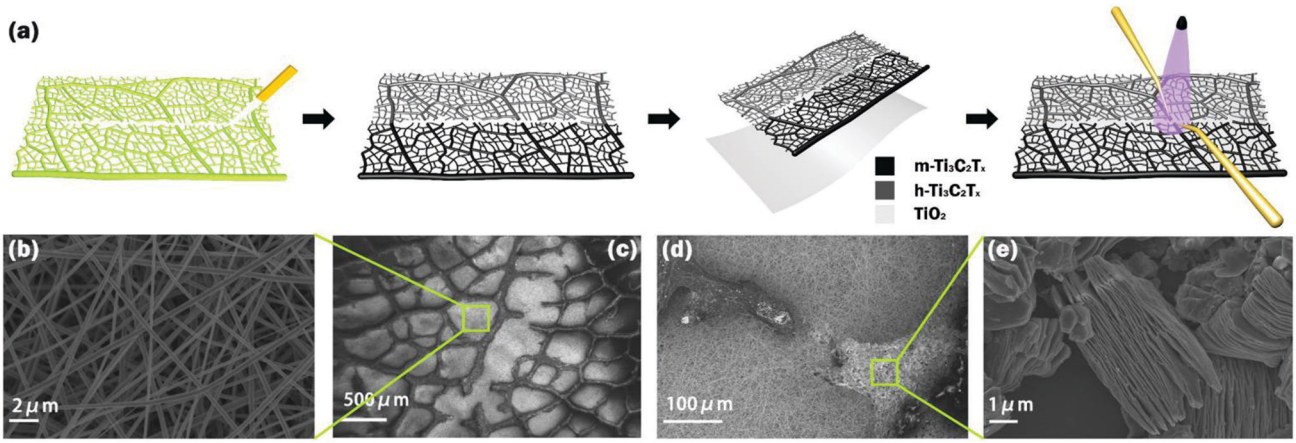

Fig. 3 (a) Schematic illustration of the photodetector integration process. (b) Enlarged SEM image of electrospun TiO_2 films of the UV photodetector. (c) SEM image of the UV photodetector. (d) Enlarged SEM image of the local photodetector where probes are fixed during the photoelectrical measurement. (e) SEM image of h-$Ti_3C_2T_x$.

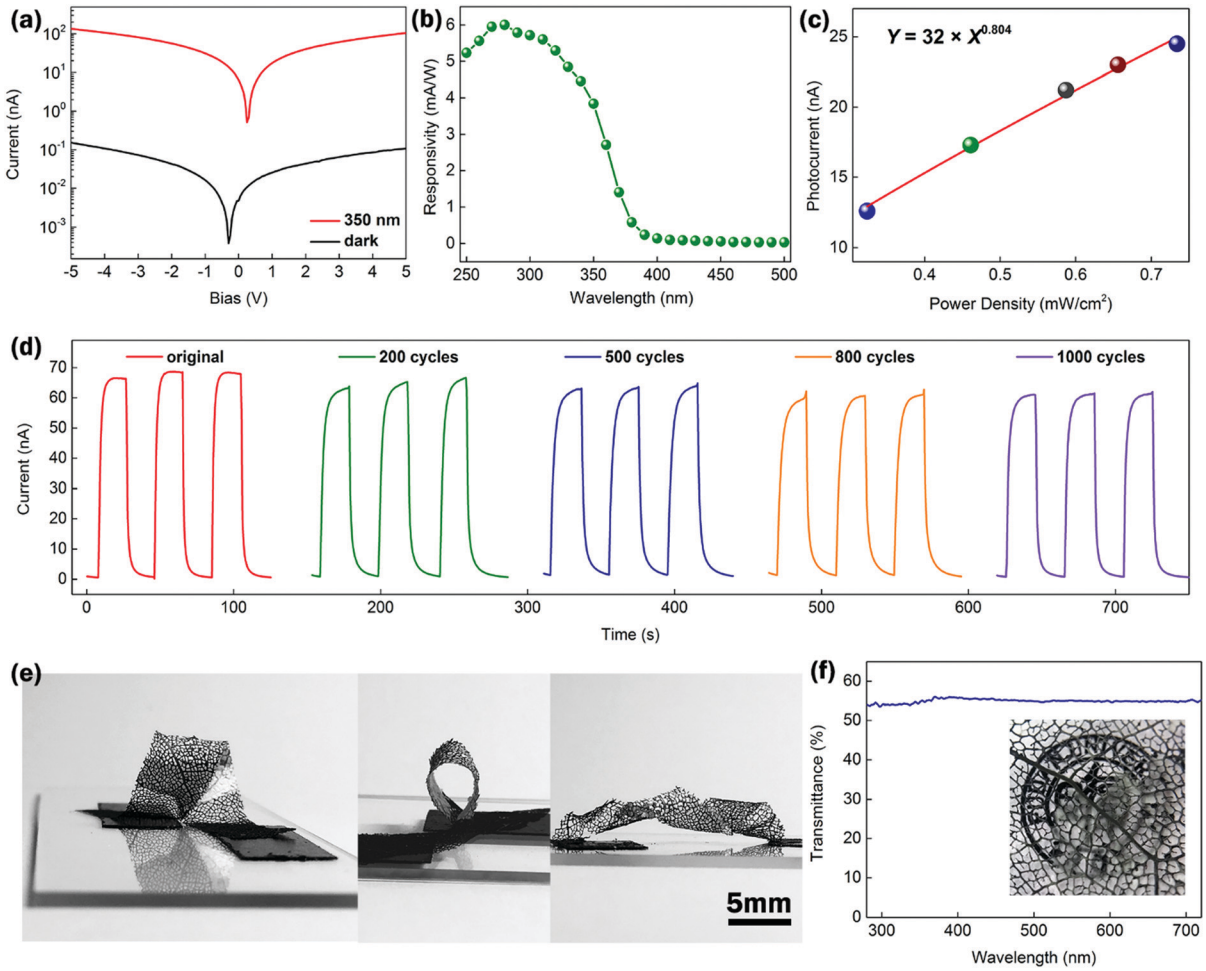

Fig. 4 Photoelectrical performance of the leaf-based UV photodetector. (a) *I–V* curves of the photodetector. 350 nm light intensity: 0.676 mW cm^{-2}. (b) Responsivity at 5 V bias under irradiation with different wavelengths. (c) *I–P* fitting relationship. (d) *I–t* curves at 5 V bias under 350 nm illumination after being bent for different cycles. (e) Optical images of flexible UV photodetectors attached to a glass slide, which are bent into a ring and a helix. (f) Transmittance of the leaf-based UV photodetector and the inset is the photo of the semi-transparent photodetector.

reaches nearly 10^3, and the responsivity reaches 6 mA W^{-1} at 5 V (Fig. 4b). The detectivity (D^*) of the photodetector is also calculated and shown in Fig. S13 (ESI†). The relationship between the photocurrent and power density under a 5 V bias was also studied as shown in Fig. 4c and fitted as:

$$I = 32 \times P^{0.804}$$

where I is the photocurrent (nA) and P represents the power density. The linear *I–V* curves demonstrate that TiO_2 and the two kinds of $Ti_3C_2T_x$ can form typical Ohmic contacts (Fig. S15, ESI†), which is also confirmed through the ultraviolet photoelectron spectroscopy (UPS) data in Fig. S14 (ESI†). The work functions of m-$Ti_3C_2T_x$ and h-$Ti_3C_2T_x$ are 4.33 eV and 3.71 eV, which are lower than the work function of anatase TiO_2,[31–33] meaning there is no blocking layer between TiO_2 and the electrodes. It is worth noting than the two kinds of MXenes have dissimilar work functions, which may result from their different surface chemistry[34] and the mechanism needs further exploration.

As Fig. 4d shows, the rise/fall time of the photodetector before bending tests is 2.27/2.54 s. The photodetector exhibits quite a stable UV response under 350 nm illumination at 5 V bias; even after being bent at 180° for 0–1000 times the photocurrent still maintains over 90% of the value at the original state. It should be noted that this free-standing photodetector has excellent flexibility as exhibited in Fig. 4e. In this scenario the photodetector can be easily bent to a ring or a helix, thanks to the ultraflexibility of the leaf electrode and TiO_2 film. In addition, it can be seen from the image that the electrode and TiO_2 film are in good contact, indicating its potential of working under different circumstances. Furthermore, it is found that the photodetector is semi-transparent (Fig. 4f) with a transmittance of nearly 60%.

In summary, a highly transparent flexible free-standing electrode with rather low resistance and tunable work function is successfully prepared. The transparent electrode is based on a leaf vein network coated with a highly conductive MXene layer, achieving a transmittance of about 90% with a wide range of sheet resistance values, of which the minimum 3 Ω sq^{-1} is realized. Additionally, the electrode is endowed with excellent flexibility and stability, which maintains good conductivity after

1000 bending cycles and survives a 50 times tape test as well as a crumpling test. Meanwhile, to depict the function of the leaf-based electrode in a much more specific way, a free-standing semi-transparent UV photodetector was constructed using the electrode and flexible electrospun TiO_2 films. The photodetector exhibits outstanding flexibility with a clear photoresponse, of which the photocurrent maintains 90% after being bent for 1000 times. What's more, it can be bent into a ring or a helix and keep good contact between the electrode and TiO_2, showing the ability to adapt to various scenarios.

Conflicts of interest

There are no conflicts to declare.

Acknowledgements

We thank Dr Yong Zhang and Jinwen Pan for discussions and experimental and technical assistance. This work was funded by National Key R&D Program of China (No. 2018YFA0703700), National Natural Science Foundation of China (No. 51872050 and 11674061), Ministry of Education Joint Fund for Equipment Pre-Research (No. 6141A02033241), and Science and Technology Commission of Shanghai Municipality (No. 19520744300, 18520710800, and 18520744600). Part of the research was carried out in Fudan Nanofabrication Laboratory.

References

1 B. Han, Q. Peng, R. Li, Q. Rong, Y. Ding, E. M. Akinoglu, X. Wu, X. Wang, X. Lu, Q. Wang, G. Zhou, J. M. Liu, Z. Ren, M. Giersig, A. Herczynski, K. Kempa and J. Gao, *Nat. Commun.*, 2016, **7**, 12825.
2 S. Chen, Z. Fu, H. Zhang, D. Legut, T. C. Germann, Q. Zhang, S. Du, J. S. Francisco and R. Zhang, *Adv. Funct. Mater.*, 2018, **28**, 1804867.
3 Y. Ma, N. Liu, L. Li, X. Hu, Z. Zou, J. Wang, S. Luo and Y. Gao, *Nat. Commun.*, 2017, **8**, 1207.
4 F. Shahzad, M. Alhabeb, C. B. Hatter, B. Anasori, S. Man Hong, C. M. Koo and Y. Gogotsi, *Science*, 2016, **353**, 1137–1140.
5 W. Deng, H. Huang, H. Jin, W. Li, X. Chu, D. Xiong, W. Yan, F. Chun, M. Xie, C. Luo, L. Jin, C. Liu, H. Zhang, W. Deng and W. Yang, *Adv. Opt. Mater.*, 2019, **7**, 1801521.
6 Y. Yang, J. Jeon, J.-H. Park, M. S. Jeong, B. H. Lee, E. Hwang and S. Lee, *ACS Nano*, 2019, **13**, 8804–8810.
7 D. Huang, Y. Xie, D. Lu, Z. Wang, J. Wang, H. Yu and H. Zhang, *Adv. Mater.*, 2019, **31**, 1901117.
8 W. Feng, R. Wang, Y. Zhou, L. Ding, X. Gao, B. Zhou, P. Hu and Y. Chen, *Adv. Funct. Mater.*, 2019, **29**, 1901942.
9 Y. Fang, Z. Liu, J. Han, Z. Jin, Y. Han, F. Wang, Y. Niu, Y. Wu and Y. Xu, *Adv. Energy Mater.*, 2019, **9**, 1803406.
10 K. Hantanasirisakul and Y. Gogotsi, *Adv. Mater.*, 2018, **30**, 1804779.
11 M. Naguib, M. Kurtoglu, V. Presser, J. Lu, J. Niu, M. Heon, L. Hultman, Y. Gogotsi and M. W. Barsoum, *Adv. Mater.*, 2011, **23**, 4248–4253.
12 C. Couly, M. Alhabeb, K. L. Van Aken, N. Kurra, L. Gomes, A. M. Navarro-Suárez, B. Anasori, H. N. Alshareef and Y. Gogotsi, *Adv. Electron. Mater.*, 2018, **4**, 1700339.
13 C. J. Zhang, B. Anasori, A. Seral-Ascaso, S. H. Park, N. McEvoy, A. Shmeliov, G. S. Duesberg, J. N. Coleman, Y. Gogotsi and V. Nicolosi, *Adv. Mater.*, 2017, **29**, 1702678.
14 K. Rasool, M. Helal, A. Ali, C. E. Ren, Y. Gogotsi and K. A. Mahmoud, *ACS Nano*, 2016, **10**, 3674–3684.
15 A. Agresti, A. Pazniak, S. Pescetelli, A. Di Vito, D. Rossi, A. Pecchia, M. Auf der Maur, A. Liedl, R. Larciprete, D. V. Kuznetsov, D. Saranin and A. Di Carlo, *Nat. Mater.*, 2019, **18**, 1228–1234.
16 K. Montazeri, M. Currie, L. Verger, P. Dianat, M. W. Barsoum and B. Nabet, *Adv. Mater.*, 2019, **31**, 1903271.
17 Y. Liu, H. Xiao, I. William and A. Goddard, *J. Am. Chem. Soc.*, 2016, **138**, 15853–15856.
18 Z. Kang, Y. Ma, X. Tan, M. Zhu, Z. Zheng, N. Liu, L. Li, Z. Zou, X. Jiang, T. Zhai and Y. Gao, *Adv. Electron. Mater.*, 2017, **3**, 1700165.
19 L. Yu, A. S. R. Bati, T. S. L. Grace, M. Batmunkh and J. G. Shapter, *Adv. Energy Mater.*, 2019, **9**, 1901063.
20 W. Yang, Y. Zhang, Y. J. Zhang, W. Deng and X. S. Fang, *Adv. Funct. Mater.*, 2019, **29**, 1905923.
21 S. Chertopalov and V. N. Mochalin, *ACS Nano*, 2018, **12**, 6109–6116.
22 P. Salles, D. Pinto, K. Hantanasirisakul, K. Maleski, C. E. Shuck and Y. Gogotsi, *Adv. Funct. Mater.*, 2019, **29**, 1809223.
23 T. H. Park, S. Yu, M. Koo, H. Kim, E. H. Kim, J. E. Park, B. Ok, B. Kim, S. H. Noh, C. Park, E. Kim, C. M. Koo and C. Park, *ACS Nano*, 2019, **13**, 6835–6844.
24 B. Han, Y. Huang, R. Li, Q. Peng, J. Luo, K. Pei, A. Herczynski, K. Kempa, Z. Ren and J. Gao, *Nat. Commun.*, 2014, **5**, 5674.
25 M. Alhabeb, K. Maleski, B. Anasori, P. Lelyukh, L. Clark, S. Sin and Y. Gogotsi, *Chem. Mater.*, 2017, **29**, 7633–7644.
26 F. Meng, M. Seredych, C. Chen, V. Gura, S. Mikhalovsky, S. Sandeman, G. Ingavle, T. Ozulumba, L. Miao, B. Anasori and Y. Gogotsi, *ACS Nano*, 2018, **12**, 10518–10528.
27 W. Li and J. Wang, *Mol. Simul.*, 2012, **38**, 1048–1054.
28 T. He, A. Xie, D. H. Reneker and Y. Zhu, *ACS Nano*, 2014, **8**, 4782–4789.
29 C. Keplinger, J.-Y. Sun, C. C. Foo, P. Rothemund, G. M. Whitesides and Z. Suo, *Science*, 2013, **341**, 984–987.
30 B. Anasori, M. R. Lukatskaya and Y. Gogotsi, *Nat. Rev. Mater.*, 2017, **2**, 16098.
31 D. O. Scanlon, C. W. Dunnill, J. Buckeridge, S. A. Shevlin, A. J. Logsdail, S. M. Woodley, C. R. Catlow, M. J. Powell, R. G. Palgrave, I. P. Parkin, G. W. Watson, T. W. Keal, P. Sherwood, A. Walsh and A. A. Sokol, *Nat. Mater.*, 2013, **12**, 798–801.
32 X. J. Xu, J. X. Chen, S. Cai, Z. H. Long, Y. Zhang, L. X. Su, S. S. He, C. Q. Tang, P. Liu, H. S. Peng and X. S. Fang, *Adv. Mater.*, 2018, **30**, 1803165.
33 G. Xiong, R. Shao, T. C. Droubay, A. G. Joly, K. M. Beck, S. A. Chambers and W. P. Hess, *Adv. Funct. Mater.*, 2007, **17**, 2133–2138.
34 A. Agresti, A. Pazniak, S. Pescetelli, A. Di Vito, D. Rossi, A. Pecchia, M. Auf der Maur, A. Liedl, R. Larciprete, D. V. Kuznetsov, D. Saranin and A. Di Carlo, *Nat. Mater.*, 2019, **18**, 1228–1234.